Ore Geology Reviews 143 (2022) 104783

Contents lists available at ScienceDirect

Ore Geology Reviews

journal homepage: www.elsevier.com/locate/oregeorev

Textural indicators of mineralisation potential in porphyry magmatic systems – A framework from the archetypal Yerington district, Nevada

Lawrence C. Carter *, Ben J. Williamson

Camborne School of Mines, University of Exeter, Cornwall TR10 9FE, UK

ARTICLE INFO

Keywords:
Porphyry deposits
Magmatic-hydrothermal transition
Fluid exsolution
Miarolitic cavities
USTs
Undercooling

ABSTRACT

Porphyry-type deposits are spatially and temporally associated with the relatively shallow and texturally complex parts of magmatic systems. Whilst certain textures offer snapshots into the physical processes which result in fluid exsolution and hydrothermal mineralisation, their documentation and interpretation remains disjointed. To address this, we describe a suite of magmatic and magmatic-hydrothermal textures from the classic Yerington Cu (-Mo-Au) porphyry district, Nevada, where Cenozoic extension and tilting has exposed a unique, ~8 km palaeodepth, cross-section through the magmatic system. Within the granite cupolas that underlie the Ann Mason and Yerington porphyry deposits, these textures include pegmatitic pods and massive silica bodies. Emplaced through the cupolas, and genetically associated with ore formation, are aplite dykes that host mineralised unidirectional solidification textures (USTs), pegmatitic segregations, miarolitic cavities and early A-type quartz veins. Based on field relations, including associations with hypogene mineralisation, petrography and Ti-in-quartz crystallisation temperatures, we highlight how these textures may record the timing and location of the magmatic-hydrothermal transition and ore-formation. By doing so we provide a textural framework for exploration geologists to assess the likely 3D spatial and temporal architecture of porphyry mineralisation at the district-prospect scale before employing more invasive and expensive techniques.

1. Introduction

Porphyry-type deposits have a strong spatial and temporal association with dioritic to granitic intrusions (Sillitoe, 2010). Magmas crystallising at relatively deep crustal levels usually acquire a relatively homogenous/equigranular equilibrium texture that reveals little about their nature and evolution (Candela, 1997). In contrast, magmatic rocks genetically associated with magmatic-hydrothermal mineralisation tend to have more complex disequilibrium textures, typically containing porphyritic, aplitic and pegmatitic domains, miarolitic cavities, unidirectional solidification textures (USTs), massive silica bodies, quartz eyes, graphic and micrographic intergrowths and dendritic, acicular and/or skeletal crystals (e.g. Fenn, 1986; Kirkham and Sinclair, 1988; London, 1992; Candela, 1997; Kirwin, 2005; London and Morgan, 2012). These features are indicative of some of the numerous physical and chemical factors which may lead to magmatic-hydrothermal mineralisation, including: chemical evolution of magmas to more water- and ore-element-rich compositions (e.g. Rohrlach and Loucks, 2005; Richards, 2011); relatively rapid ascent into reservoirs at ~ 2–5 km depths causing undercooling; the exsolution of sufficient volumes of magmatic-hydrothermal fluids, and focussing of these fluids into relatively narrow zones of mineralisation (Candela, 1997; Richards, 2005; Sillitoe, 2010; Wilkinson, 2013). Further, the observation and interpretation of such textures offers first-order tools for field geologists to understand the ore-forming potential of different magmatic systems and their component parts.

Despite the invariable association of these textures with porphyry-style mineralisation, their documentation and interpretation remains disjointed and fragmentary. This could be because of their small size (often less than several cm in size, requiring close inspection of outcrop and/or drill core for identification), often poor preservation due to overprinting by subsequent magmatic-hydrothermal and hydrothermal processes, lack of recognition and insufficient exposure of the sub-ore root-zones of porphyry deposits in the vast majority of magmatic-hydrothermal systems (Seedorff et al., 2008). To address this, we describe a suite of magmatic-hydrothermal textures from the archetypal Yerington Cu(-Mo-Au) porphyry district, Nevada, where Cenozoic extensional faulting has exposed an exceptional ca. 8 km deep cross-

* Corresponding author.
E-mail address: l.c.carter@exeter.ac.uk (L.C. Carter).

https://doi.org/10.1016/j.oregeorev.2022.104783
Received 23 November 2021; Received in revised form 31 January 2022; Accepted 15 February 2022
Available online 17 February 2022

section through the porphyry system, from the volcanic terrane down through a number of porphyry centres to their plutonic root zones (Proffett and Dilles, 1984; Dilles, 1987). We discuss the genesis of these textures and their significance in exploration.

2. Geological setting - the Yerington porphyry system, Nevada

Late Cenozoic basin and range extensional faulting and associated fault block rotation has exposed a unique < 1 to ~ 8 km palaeodepth cross-section through the middle Jurassic composite Yerington batholith, including volcanic rocks, plutons, and several porphyry centres (Proffett, 1977; Hudson and Oriel, 1979; Proffett and Dilles, 1984; Dilles, 1987; Dilles and Wright, 1988; Dilles and Proffett, 1995). The Yerington batholith was emplaced into Triassic to Jurassic intermediate composition volcanics, volcaniclastic and argillaceous sedimentary rocks, and basal exposures of the Jurassic Artesia Lake Volcanics, which are unconformably overlain by the Jurassic latitic Fulstone Spring Volcanics (Dilles, 1987; Dilles and Wright, 1988; Proffett, 2007), see reconstructed (pre-tilt) cross-section in Fig. 1 (Dilles, 1987; Schöpa et al., 2017).

The batholith comprises three main plutonic phases, which, listed in order of increasing emplacement depth, are: 1) the McLeod Hill quartz monzodiorite, 2) Bear quartz monzonite, and 3) Luhr Hill granite (Dilles, 1987). These are cross-cut by swarms of granite-composition porphyry and aplite dykes which where emplaced through cupolas at the top of the underlying Luhr Hill granite (Proffett, 1977; Dilles, 1987; Carter et al. 2021a, Carter et al., 2021b). The dyke swarms are spatially and temporally associated with the batholith's four known porphyry copper deposits: Ann Mason; Yerington; MacArthur and Bear (Fig. 1) (e.g. Proffett, 1979; Dilles, 1987; Dilles and Proffett, 1995). Combined, these host measured and indicated resources in excess of 9 Mt of contained Cu (Dilles and Proffett, 1995; Bryan, 2014; Henderson et al., 2014; Hudbay Minerals Inc., 2021).

The uniquely exposed cross section through the Yerington porphyry system provides a rare opportunity to study the root zones beneath the district's porphyry deposits and textural evidence for the magmatic-hydrothermal transition (Carter et al., 2021b), which is seldom exposed elsewhere (Seedorff et al., 2008).

3. Methods

This article is based on first-order field observations of cross-cutting relationships, disequilibrium phenomena and textures indicative of fluid exsolution in outcrop from across the Yerington porphyry district, Nevada, and from several kilometres of drill core through the Ann Mason and Yerington porphyry deposits. These observations were supplemented by microscale petrographic and geochemical analyses of quartz USTs. The analytical methods used are described below and in more detail in Carter et al. (2021b).

3.1. SEM-EDX-CL

Selected samples of quartz USTs from outcrop and drill core were prepared as polished thin sections (30 μm thickness) for microscale analysis. Following optical microscopy, section surfaces were carbon coated to a thickness of around 25 nm using an Emitech K950 carbon coater. Scanning electron microscope (SEM)-based backscattered electron (BSE) and cathodoluminescence (CL) imaging and qualitative energy dispersive X-ray (EDX) elemental mapping were carried out using an FEI Quanta 650 Field Emission Gun-SEM equipped with a Gatan monochrome CL detector and 2x Bruker SDD EDS detectors (XFlash series 6 | 30) at the University of Exeter's Environment and Sustainability Institute. The instrument was operated at an accelerating voltage of 20 kV. Elemental maps were obtained using a minimum of 4 scans and a dwell time of 32 μs, and processed using Bruker Esprit software version 1.9a. The CL images were collected from single scans with a 30 μs dwell time, a processing resolution of 3072 × 2048 pixels and 256 grey levels. CL brightness and contrast were optimized to reveal inhomogeneities in quartz; other phases therefore appear either white or black. In the SEM-CL images, the different grey levels shown by quartz represent different

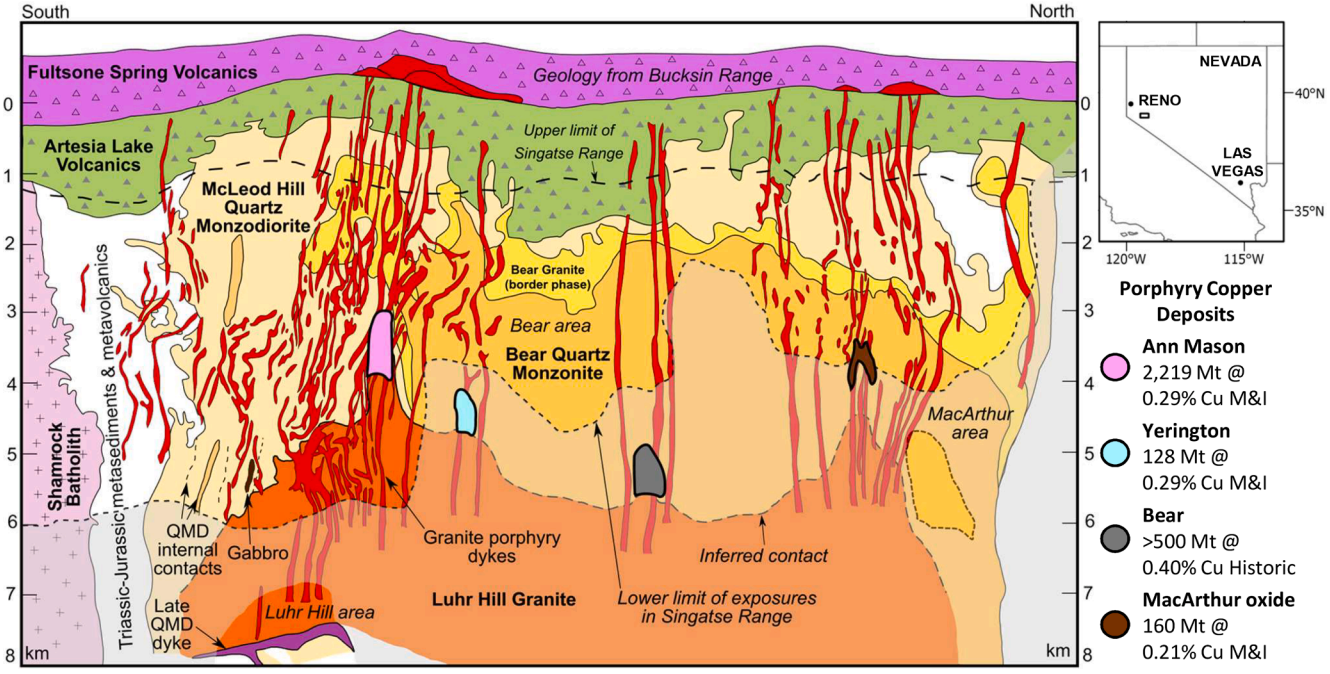

Fig. 1. Pre-tilt cross section through the Yerington District, Nevada, reconstructed to a palaeo-depth of 8 km, showing the intrusive units of the Jurassic Yerington batholith, including the various generations of porphyry dyke swarms which were emplaced through apophyses of the Luhr Hill granite, the district's four known porphyry copper deposits (Yerington and Bear deposits projected onto section) and overlying volcanics. Section from Dilles (1987) and Schöpa et al. (2017), with resource estimates from Bryan (2014), Dilles and Proffett (1995), Henderson et al. (2014) and Hudbay Minerals Inc. (2021). QMD = quartz monzodiorite, M&I = measured & indicated, historic = non-compliant historic estimate.

luminescence colours that can be attributed to defects in the lattice and/or the presence of trace elements in the crystal structure (Müller et al., 2010).

3.2. QEMSCAN®

The mineralogy of selected carbon-coated polished thin sections was determined using a QEMSCAN® 4300 automated mineralogical assessment system at Camborne School of Mines (Gottlieb et al., 2000; Goodall et al., 2005; Goodall and Scales, 2007). The system is based on a Zeiss Evo 50 SEM with 4 × Bruker SDD EDS detectors (XFlash) controlled by iMeasure v. 4.2SR1 software for data acquisition and iDiscover v. 4.2SR1 and 4.3 for spectral interpretation and data processing (Rollinson et al., 2011). The QEMSCAN® was operated at an accelerating voltage of 25 kV and a beam current of 5 nA, with a working distance of around 22 mm, in high vacuum mode and with automatic beam calibration every 30 min. Fieldscan measurement mode was used to obtain a mineralogical map of nearly the whole polished section area (39 × 20 mm) at an analytical point resolution, or pixel spacing, of 10 μm and with 1000 X-ray counts per pixel. The data from each point of analysis was automatically compared with a Species Identification Protocol (SIP) database of mineral and non-crystalline phase spectra to identify the minerals present. The SIP used was modified from the LCU5 SIP provided with the QEMSCAN®, which includes a range of oxide, sulphate, and silicate minerals. All mineral categories were checked by manually assessing elemental abundances, element ratios, and BSE signal. A boundary phase post processor was applied to reduce edge effects and to resolve rogue pixels. Data collection and processing followed in house QA/QC procedures. The data were output as mineralogical maps (Fig. 6b, Supplementary Data 1) and in a mineral associations matrix (Supplementary Data 1).

3.3. EPMA

Concentrations of Al, Ti and Fe in quartz were determined by electron probe microanalysis (EPMA) using a JEOL JXA-8200 electron microprobe at Camborne School of Mines, University of Exeter. The thin sections used for the SEM studies were re-polished and carbon coated to a thickness of around 25 nm using an Emitech K950 carbon coater. The instrument was operated at an accelerating voltage of 20 kV, a beam current of 70 nA and a spot size of 15 μm. This relatively large spot size was used due to the sensitivity of quartz at high current and with a narrow beam (Kronz et al., 2012). SiO_2 was assumed to be 100%. Corundum (Geo MkII), rutile and hematite (Astimex) calibration standards were used for Al, Ti and Fe, respectively. For calibration at low concentrations or as 'blank'-control, some studies use a synthetic doped or pure SiO_2-glass. This was deemed inappropriate as the behaviour of these materials during electron irradiation is very different to that of quartz (e.g. Kronz et al., 2012). Peak and background measurement count times were both 200 s. Limits of detection (LOD) were (2σ) 30 ppm for Al, 28 ppm for Ti and 28 ppm for Fe. To estimate precision, we undertook seven repeat analyses of a single homogenous, magmatic, un-zoned (from SEM-CL imaging) quartz crystal from within a polished section of Luhr Hill granite (sample YM33b in Supplementary Data 2). The mean, range and 1 s.d. of these were: Al (78; 51–101; 20 ppm); Ti (81; 70–91; 8 ppm); Fe (39; 28–52; 12 ppm). From these we used ± 1 s.d to express our analytical uncertainties: Al ± 20 ppm; Ti ± 8 ppm; Fe ± 12 ppm.

3.4. Ti-in-quartz geothermometry

Using the EPMA data (Supplementary Data 2), Ti-in-quartz geothermometry (TitaniQ, method of Wark and Watson, 2006) was used to assess the crystallisation temperatures of quartz USTs. Based on the consistent presence of titanite in the USTs' inter quartz aplite layers, the activity of TiO_2 ($aTiO_2$) was assigned a value of 0.7, in line with other studies (e.g. Claiborne et al., 2010; McDowell et al., 2014), including specific studies on the Yerington District (Dilles et al., 2015; Carter et al., 2021b). We acknowledge that the $aTiO_2$ may have changed during the evolution and crystallisation history of the system, but we assume that this was negligible given that the same Ti-bearing minerals (notably titanite and trace rutile, see Supplementary Data 1) are present in the compositionally similar granite and aplite dykes. Further, as discussed in Carter et al. (2021b), small changes in the $aTiO_2$ will have a minor effect on the calculated crystallisation temperature. To estimate precision, we calculated TitaniQ for seven repeat EPMA analyses of a single homogenous, magmatic, un-zoned quartz phase within the Luhr Hill granite (sample YM33b in Supplementary Data 2). From this, we determined an uncertainty in our geothermometry data of around ± 13 °C.

4. Results and discussion

4.1. Massive silica bodies and pegmatitic pods

The exposed Luhr Hill granite cupola in Mason pass, which lies just below (palaeo-vertically) the Ann Mason porphyry Cu(-Mo-Au) deposit (Dilles, 1987), is relatively uniform in appearance, notwithstanding the products of pervasive subsequent hydrothermal alteration (Dilles et al., 2000; Halley et al., 2015). The Luhr Hill granite intruded, and has sharp contacts with, the McLeod Hill quartz monzodiorite, but this caused no visible signs of contact metamorphism or metasomatic alteration. In addition, there is no documented or observable textural evidence for the exsolution of mineralising fluids in the Luhr Hill granite cupola such as ore-mineral-bearing miarolitic cavities or internally sourced veins (Carter et al., 2021b). Instead there are rare pegmatitic pods and orbs (Fig. 2a) which are often tens of cm in diameter, have an almost anhydrous mineralogy (quartz, K-feldspar, plagioclase, accessory titanite and Fe-oxides, and only trace biotite), no cavities, are unmineralised, isolated (i.e. are not connected to or associated with veins), and have no adjacent alteration (Carter et al., 2021b). It is likely that these formed as a result of magmatic processes, rather than involving hydrothermal fluids, because: i) they show inward-growing micro-graphic texture at their margins which is unique to the crystallisation of undercooled, non-H_2O-saturated, silicate (i.e. magmatic) liquids/melts (Fenn, 1986; London, 1992; London and Morgan, 2012); ii) they show comparable Ti-in-quartz crystallisation temperatures to their host granite (~730 °C; Carter et al., 2021b); iii) such graphic texture is not found in hydrothermal veins which form by the precipitation of minerals from a predominantly aqueous fluid (London and Morgan, 2012); and iv) from experimental studies, the formation of pegmatitic and graphic textures does not require water saturation (e.g. Fenn, 1986; London, 1992).

An alternative explanation for such pegmatitic pods is that they represent pockets of fluid which exsolved upon emplacement of the magma. Such fluids, however, cannot have contained enough solutes to completely mineralise the pockets themselves, and it is difficult to envisage how they could have been subsequently infilled unless they were open to through-flowing hydrothermal fluids. The latter, however, is likely to have resulted in lower Ti-in-quartz temperatures compared with those in the surrounding granites. In addition, their 'granite'-like quartz-K-feldspar-plagioclase assemblage is more indicative of crystallisation from a silicate liquid/melt.

Massive silica bodies (Fig. 2b) (nomenclature after Kirwin, 2005) also outcrop in the exposed cupola, close to the pegmatitic pods. Whilst their borders are obscured in outcrop, these rounded masses are several metres in diameter, are isolated (i.e. not associated with veins), show no hydrothermal banding, and do not host hypogene or secondary Cu mineralisation, although they do show Fe-oxide staining. As their margins are not exposed, it is possible that they have a feldspar-rich outer zone, but this cannot be confirmed. The most obvious heterogeneity within the silica bodies is rare small quartz-filled cavities (Fig. 2b inset), usually < 5 cm in diameter.

Given their textural similarities and spatial association, the massive

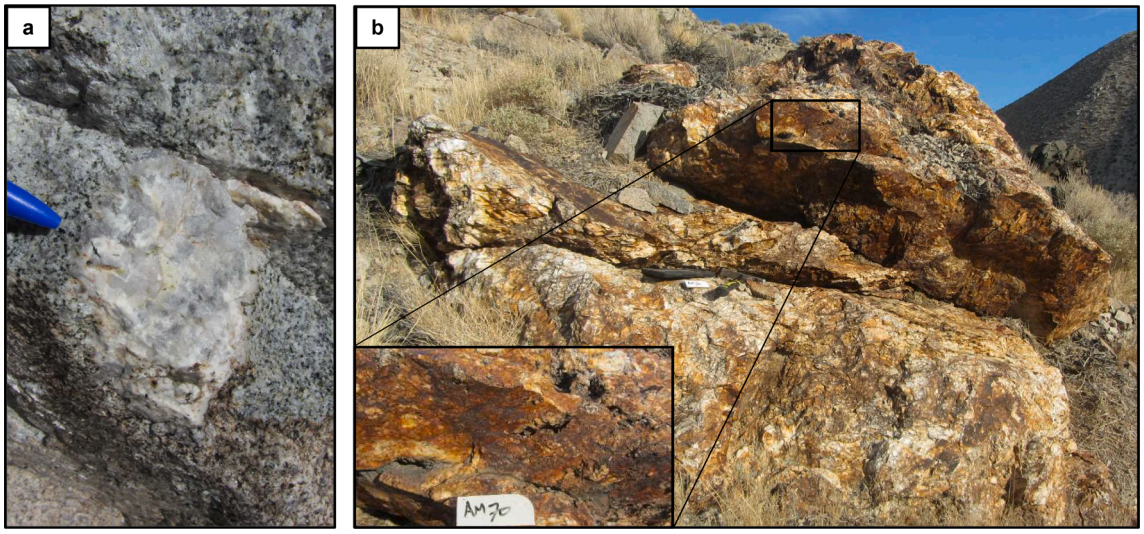

Fig. 2. a, Field photograph of a quartz-feldspar pegmatitic pod in the exposed cupola of the Luhr Hill granite. Pen lid for scale. b, Field photograph of a massive silica body (nomenclature after Kirwin, 2005) in the exposed cupola of the Luhr Hill granite, palaeo-vertically beneath the Ann Mason porphyry deposit (Dilles, 1987). The body contains no hydrothermal banding or recrystallisation textures and is not mineralised. Hammer and label for scale. Inset; Quartz lined cavities within the silica body. These contain only quartz and constitute an insignificant volume of the body. Label for scale.

silica bodies and pegmatitic pods likely formed due to the same magmatic phenomena, although at different scales. Their development is probably related to intense undercooling (London, 1992), defined as 'the difference between the temperature at which the melt saturates with respect to a mineral and the temperature at which the mineral actually nucleates and grows', which usually results from the rapid upward emplacement of magmas into a cooler environment (Candela, 1997). Undercooling also exerts a significant influence on crystal growth rate and morphology, and therefore the resultant textures (Swanson, 1977).

4.2. Macro textures of the magmatic-hydrothermal transition

Swarms of porphyry dykes cross-cut and appear to have been focussed through apophyses of the Luhr Hill granite cupola. Whilst many are transected by A-, AB- and B-type (nomenclature after Gustafson and Hunt, 1975) and later quartz veins, in both outcrop and drill core, no direct textural evidence could be found for the exsolution of mineralising fluids (e.g. miarolitic cavities), and there is none reported in the literature. They do contain ore minerals, however, so are likely to have been mineralised by fluids from elsewhere.

Several generations of aplite dykes also appear to have been focused through the same apophyses. These vary from several cm to a few m in width and have complex cross-cutting relations between different generations. The aplite and porphyry dykes occasionally show evidence of mingling, which indicates that emplacement, of at least some generations, was contemporaneous (Carter et al., 2021a). Significantly, these aplite dykes are pegmatitic, interfinger with quartz segregations, host quartz USTs and mineralised miarolitic cavities, and are internally veined or cut by mineralised A- and B-type quartz veins. They likely have affinities with aplitic 'vein dykes' previously described elsewhere (e.g. Spurr, 1923), such as at the Henderson Mo porphyry system (White et al., 1981; Shannon et al., 1982; Kirkham and Sinclair, 1988).

The pegmatitic segregations in the aplite dykes are predominantly composed of masses of coarse K-feldspar and quartz crystals up to several cm long. They occur in aplite dykes within the porphyry deposits and in the upper (cupola) and deeper portions of the underlying Luhr Hill granite (Proffett, 2007; Runyon et al., 2017). The magmas that formed them likely underwent varying degrees of undercooling (e.g. Swanson, 1977; Fenn, 1986; London, 1992; London and Morgan, 2012).

The interfingering aplite-quartz segregations (Fig. 3) vary in thickness, appearing to pinch and swell then pinch out completely. Where present, they are always at the margins of aplite dykes but also feather into their central parts. These features appear to be similar to 'parting veins', described in other magmatic-hydrothermal systems as 'quartz veins that contain numerous septa or partings of aplite' (Kirkham and Sinclair, 1988). These textures most certainly indicate the mingling of magmatic silicate liquids and hydrothermal fluids.

The quartz USTs within the aplite dykes most commonly grew inwards from nucleation points on the wall rocks, although occasionally they also appear to have grown inwards from dyke-parallel internal granite contacts (Fig. 4). They are seen in aplite dykes that cross-cut both the granite cupola and porphyry dykes, including varieties that host embayed quartz eyes (rounded quartz phenocrysts likely to have formed due to the ease of quartz relative to feldspar nucleation and are indicative of relatively volatile-rich melts; Candela, 1997; Vasyukova et al., 2013; Fig. 4e). The USTs are localised, vary in thickness and their nucleation surfaces are often non-planar and therefore crystal growth was not always parallel.

In some parts of certain aplite dykes in the Yerington district, quartz USTs comprise of multiple, subparallel to undulating, equally spaced bands of euhedral quartz crystals interlayered with aplite (Fig. 4). The quartz grains in the coarse bands range from a few mm to a few cm in length, are parallel to sub-parallel and appear to have nucleated on and grown perpendicular to the wall rocks, as also shown by Shannon et al. (1982) in the Henderson deposit. The aplite layers range from a few mm to several cm thick and predominantly consist of quartz and feldspar which is often micrographic (Fig. 5b). The bands can be traced for several m in outcrop and show variations in crystal morphology over this scale. In some instances, the USTs are mineralised with molybdenite and chalcopyrite (Fig. 4f, g & Fig. 5). Molybdenite appears to be paragenetically early, being contained as inclusions in quartz crystals nucleated on the wall rocks. Chalcopyrite appears later, being associated with subsequent quartz layers (Fig. 4g & Fig. 5).

From scanning electron microscope-based cathodoluminescence (SEM-CL) imaging, the quartz in the aplite dyke USTs is concentrically zoned inwards from the margins (Fig. 5). Its crystallisation temperatures, based on Ti-in-quartz thermometry (using the TitaniQ, method of Wark and Watson (2006), with Ti concentrations determined by electron microprobe), are ~ 750 to > 900 °C, which is mostly higher than for quartz in the host Luhr Hill granite cupola (~730 °C, Carter et al., 2021b) (Fig. 6). This difference could be due to variations in $aTiO_2$ in the system; however, this is deemed unlikely given the comparable

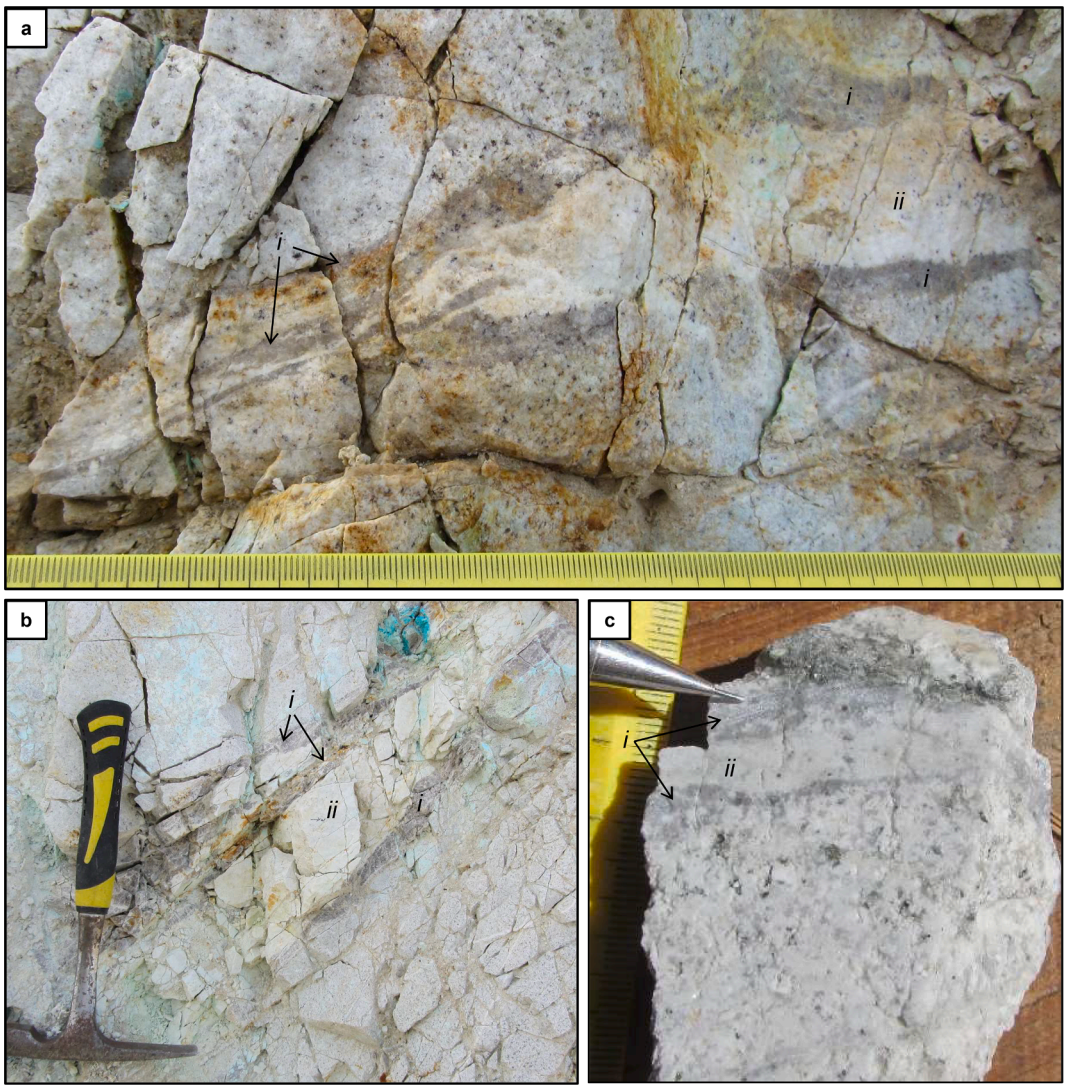

Fig. 3. a-c, Photographs of interfingering with quartz segregations (i) within aplite dykes (ii). The quartz segregations occur at the margins and within the aplite dykes. a & b are from within the Yerington Mine (Yerington porphyry deposit). c is drill core from the Ann Mason porphyry deposit. These textures are likely akin to previous descriptions of 'parting veins' in porphyry systems elsewhere (Kirkham and Sinclair, 1988).

mineralogy (notably ubiquitous presence of titanite) of the Luhr Hill granite and aplite dykes. It could also be because the highly undercooled, disequilibrium conditions under which the quartz USTs grew caused the uptake of more Ti and other trace elements into the quartz. However, assuming that the inter-UST aplite layers crystallised at the same temperature as the quartz of the UST, it is more easily explained by certain generations of aplite dykes being intruded and crystallising from melts which were relatively higher temperature than those which formed their Luhr Hill granite host, possibly originating from a deeper hotter source or having less time to cool during ascent to higher crustal levels.

The formation of USTs is understood to be linked to undercooling (London, 2009), however this alone does not explain their rhythmic texture. The repeated nature of the UST banding is likely to indicate cyclical variations in the undercooled environment of crystallisation, probably dominated by changes in pressure across cotectic boundaries between quartz-feldspar stability fields (e.g. Kirkham and Sinclair, 1988; Kirwin, 2005). This is because the quartz stability field expands with increasing pressure (Tuttle and Bowen, 1958); quartz may therefore crystallise during periods of volatile overpressure and stop when pressure declines. One possible mechanism to rapidly reduce pressure is hydraulic fracturing of the wall rocks (Candela, 1989). Upon healing of these fractures, e.g. due to mineral precipitation, pressure then builds up again and the process is repeated.

Miarolitic cavities offer the best evidence for volatile phase saturation and exsolution in the aplite dykes. To form they require bubble growth during magma ascent and decompression, and quenching of the melt during that process (Candela, 1997), before they become deformed or disappear due to flow in the magma. The miarolitic cavities, up to several cm across and often mineralised, are common within the aplite dykes which cross-cut the exposed Luhr Hill granite cupola (Fig. 7). They are characterised by euhedral quartz crystals, sometimes associated with chalcopyrite, that project into and terminate in what is likely to have been a segregation of exsolved magmatic fluids in the magma or crystal mush. The miarolitic cavities often occur in close association with USTs and pegmatitic bodies, as well as being locally connected to early-mineralised A-type veins, which are themselves cross-cut by B-type veins.

From recent micro-scale petrographic and geochemical studies of the aplite dykes from Yerington (Carter et al., 2021b), the quartz within the mineralised miarolitic cavities appears to be connected to networks of multiple quartz veinlets ('wormy quartz') in the groundmass. This 'wormy quartz' was interpreted to mark the pathways (palaeo-permeability) of exsolving mineralising fluids as well as capturing a snapshot

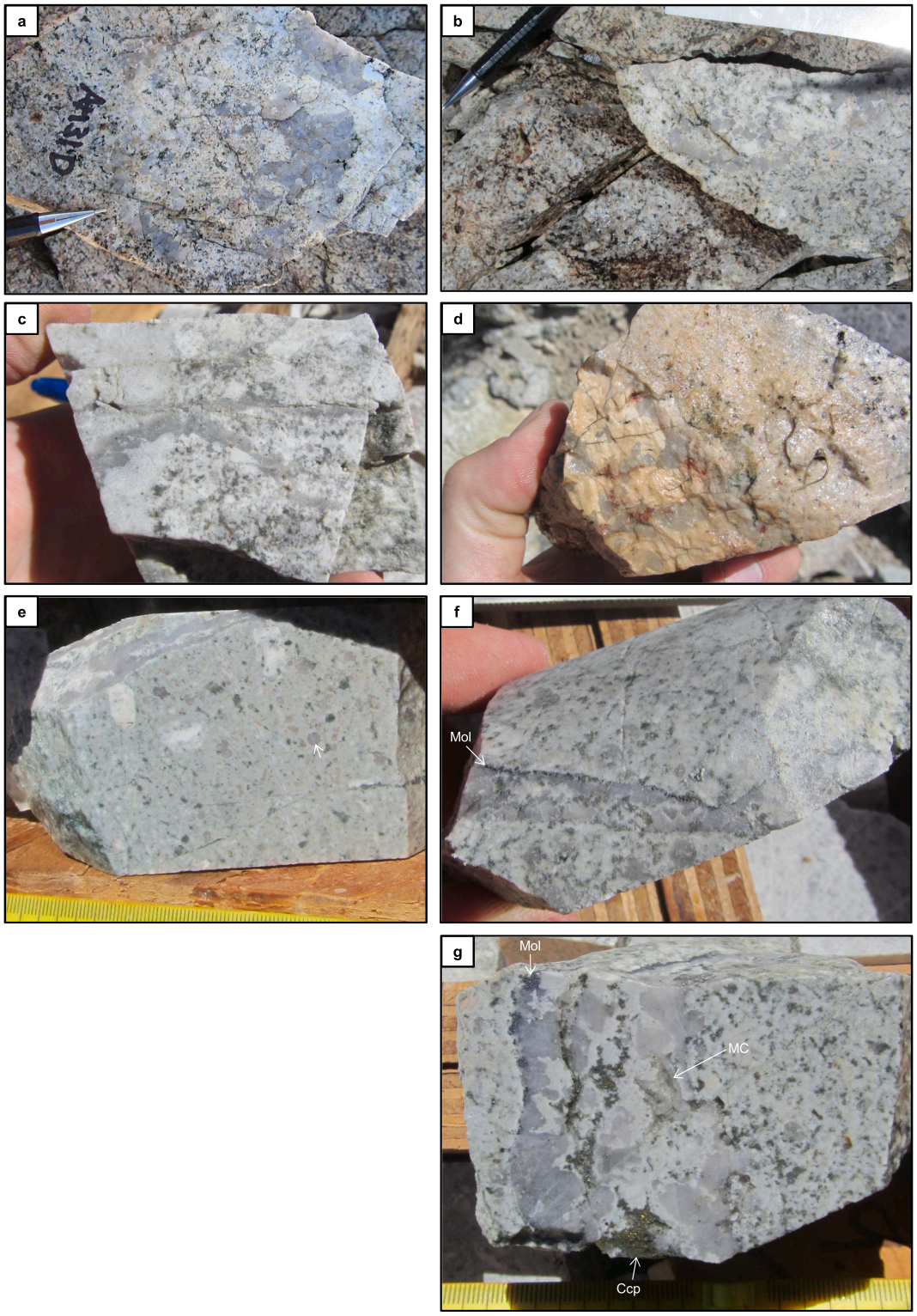

Fig. 4. Field photographs of quartz USTs in aplitic dykes in the exposed cupola region of the Luhr Hill granite (a-c) and in drill core through the Ann Mason deposit (d-g). The aplitic dykes are seen cutting the Luhr Hill granite and porphyry dykes. In e, embayed quartz eyes can be seen in the porphyry dyke (e.g. white arrow). In g, the USTs can be seen associated with miarolitic cavities (MC) and molybdenite (Mol) and chalcopyrite (Ccp) mineralisation. These aplite dykes likely have affinities with 'vein dykes' previously described elsewhere (e.g. Spurr, 1923; White et al., 1981; Shannon et al., 1982).

of the magmatic-hydrothermal transition within these 'crystal mush dykes'. By reducing effective stress (Terzaghi and Peck, 1948), the increased fluid pressure due to fluid exsolution and continued upward fluid flow through the palaeo-permeability would have triggered hydraulic fracturing of the host rock aplites and granites. This brittle failure would have caused a rapid decrease in pressure which, in turn, would have initiated the cyclic formation of USTs and magmatic quenching textures such as the rhythmically banded aplite-USTs. The exsolving mineralising fluids would have been able to exploit and permeate these micro-pathways and fractures before cooling and

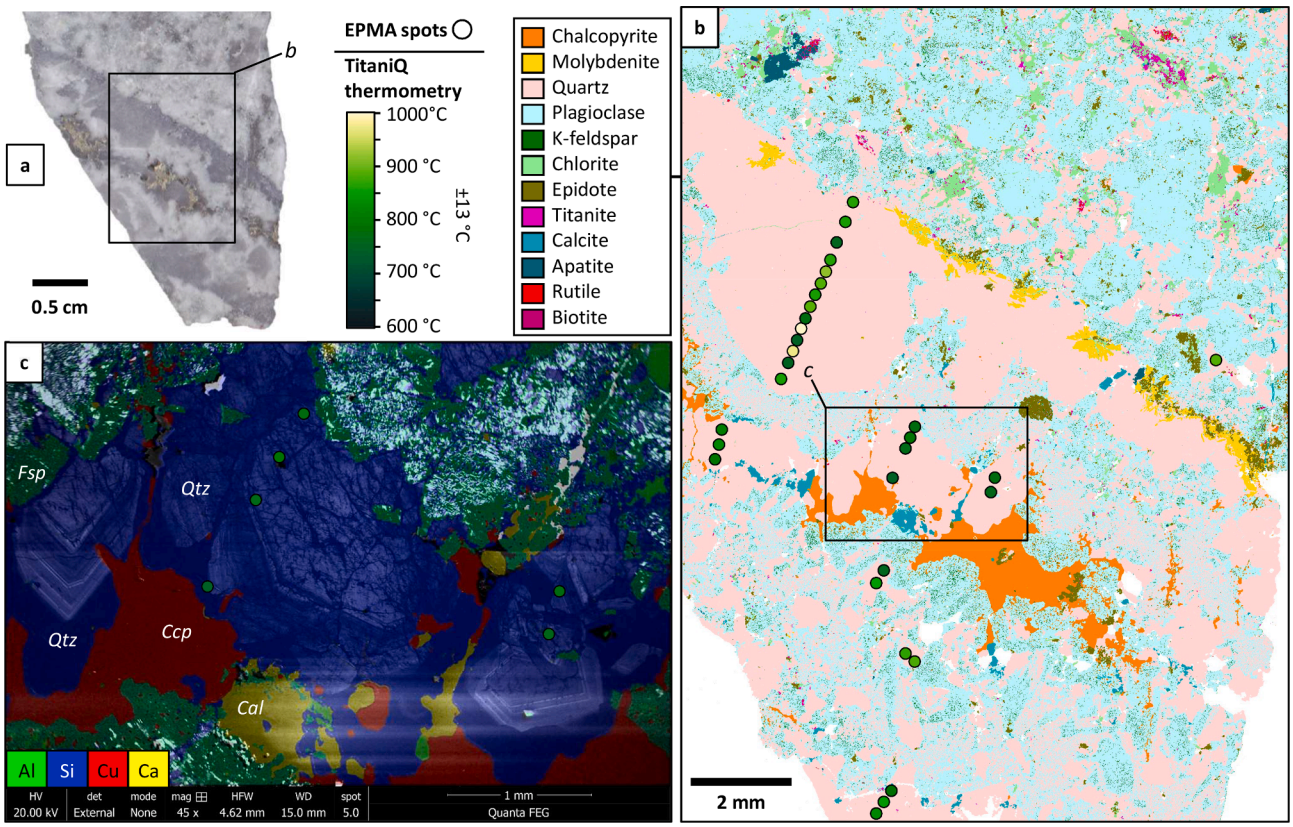

Fig. 5. a, Photograph of chalcopyrite-molybdenite-mineralised quartz USTs in an aplite dyke in drill core from the Ann Mason porphyry deposit. The top quartz UST layer marks the contact between the aplitic and host porphyry dyke. Location of b annotated; b, QEMSCAN® mineral map of the mineralised UST. Micro-graphitic texture can be seen in the aplite between the UST layers. Molybdenite is seen at the margin of the UST. Chalcopyrite is concentrated along an inner portion of the UST and is disseminated throughout the aplite. Overlain are the positions of EPMA spot analyses (spot size not representative) coloured according to Ti-in-quartz temperature (TitaniQ, method of Wark and Watson, 2006), see inset colour scale. Location of c annotated; c, SEM-CL image showing quartz zoning in the UST overlain by EDX elemental map and temperatures calculated from TitaniQ thermometry. Qtz = quartz, Fsp = feldspar, Ccp = chalcopyrite, Cal = calcite.

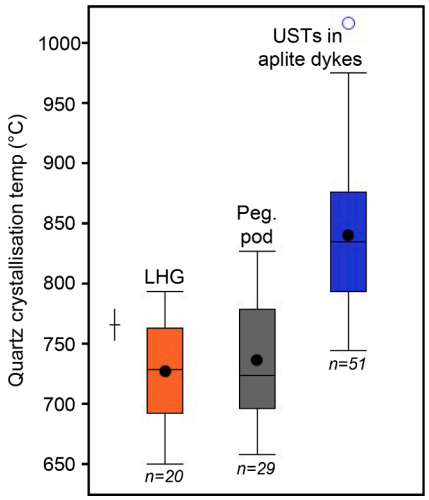

Fig. 6. Tukey box plot of Ti-in-quartz crystallisation temperature (TitaniQ, method of Wark and Watson, 2006) for Luhr Hill granite (LHG), a pegmatitic pod (peg. pod) within the Luhr Hill granite, and quartz USTs within aplite dykes from the Ann Mason porphyry deposit, which cross-cut the Luhr Hill granite cupola. n = number of analyses. Cross represents single data point uncertainty.

precipitating quartz and other minerals to produce what we now see as 'wormy quartz' and A- and B- type veins.

4.3. Magmatic-hydrothermal textures elsewhere

The textures discussed here are by no means exclusive to Yerington. USTs have also been recognised in 'Climax-type' Mo porphyry systems (e.g. White et al., 1981; Shannon et al., 1982), intrusion-related gold deposits (e.g. Kidston, Baker and Andrew, 1991; Timbarra, Mustard et al., 1988) and porphyry system-associated hydrothermal breccias (e.g. Shotgun, Rombach and Newberry, 2001), numerous Sn-W-Mo systems in Canada (e.g. Kirkham and Sinclair, 1988, who referred to them as 'comb quartz layers'), Sn mineralised granites in Tasmania (Hong et al., 2019), Cu-Au-Mo and Sn-W-Mo systems in Mongolia (Kirwin, 2005; Erdenebayar et al., 2014), and several other porphyry Au-Cu systems (e.g. North Parkes, Hithersay and Walshe, 1995; Batu Hijau, Garwin, 2002; Cadia, Wilson, 2003; Bajo de la Alumbrera, Harris et al., 2004; Ridgeway, Harris et al., 2007). We note that the documentation of USTs in Cu-rich porphyry systems in the literature appears notably rarer than for their Au- or Mo-rich counterparts. USTs within aplite dykes, or aplitic 'vein dykes' (Spurr, 1923) at Henderson (White et al., 1981; Shannon et al., 1982) have also been suggested to have a close association with hydrothermal quartz veins (Kirkham and Sinclair, 1988).

Miarolitic cavities are also documented in many other magmatic-hydrothermal ore forming systems. Examples of where they appear to be interconnected on a microscale, which may mark the pathways of exsolving magmatic-hydrothermal fluids, include the: Bajo de la Alumbrera porphyry Cu-Au deposit, NW Argentina (Harris et al., 2004); Sn-Mo-mineralised Ruby Creek granite, New South Wales, Australia; Mo-

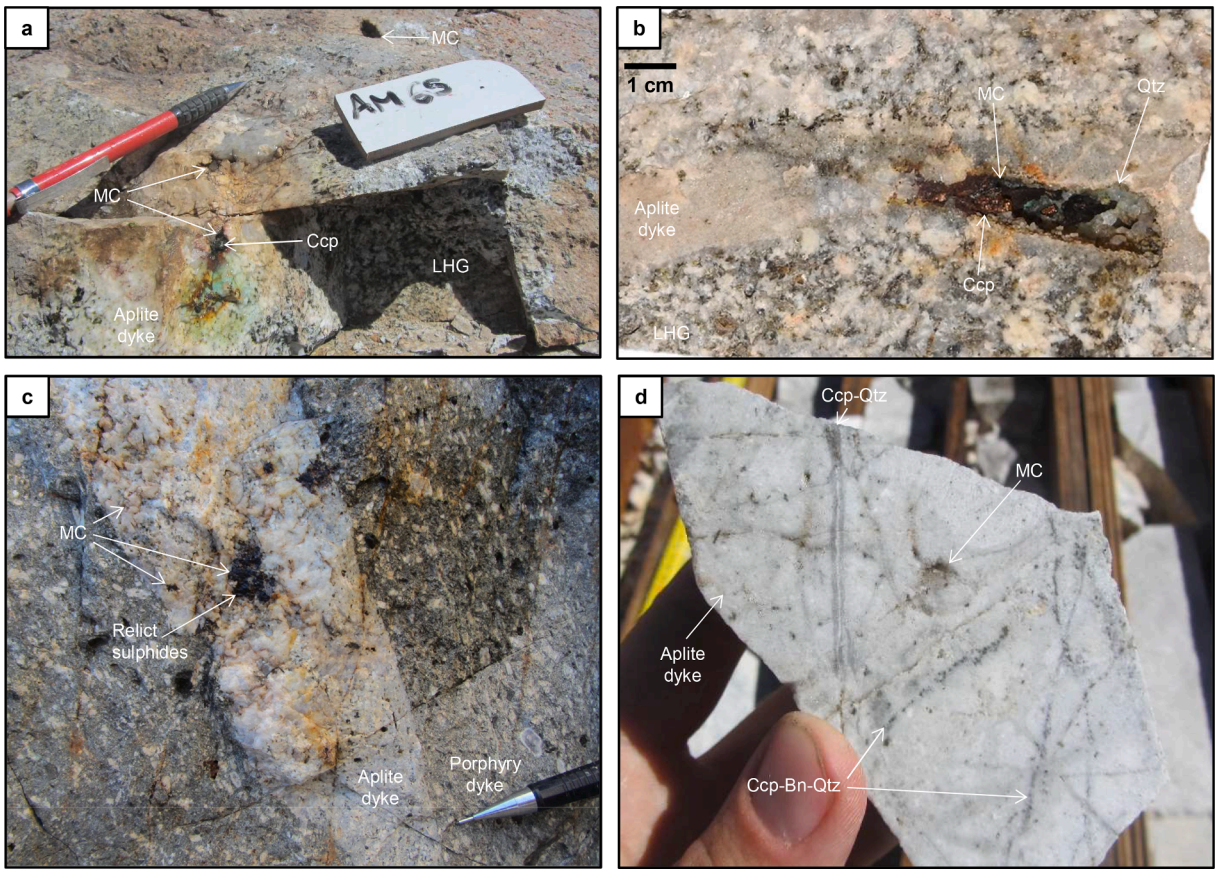

Fig. 7. a-d, Photographs of mineralised miarolitic cavities (MC) within aplite dykes which cross-cut the Luhr Hill granite (LHG). Miarolitic cavities are seen having close relationships with early chalcopyrite-bornite-quartz (Ccp-Bn-Qtz) A-type veins in d. b from Carter et al. (2021b).

mineralised leucocratic phases of the Bemboka pluton in the Lachlan fold belt of SE Australia; and Mount Morgan and the Tuckers Range Complex in Queensland, Australia, which are associated with VMS and Cu-Au mineralisation, as outlined by Candela and Blevin (1995).

Reports of massive silica bodies elsewhere include those at: Panasqueria W-Sn-Cu deposit in Portugal (Kelly and Rye, 1979); Ravenswood porphyry Cu-Mo-Au district in Queensland, Australia, with a notably large example called the 'White Blow' (Clarke, 1969); and several Mongolian magmatic-hydrothermal ore-forming systems (e.g. Kirwin, 2005; Tungalag et al., 2019). In the latter, numerous spectacular examples are exposed at Zuun Mud (porphyry Mo-Cu), South Gobi, where massive silica bodies within with the top levels of a granitic cupola are seen to transition, over several metres, directly into quartz UST layers (Kirwin pers. comm., 2021).

4.4. *Exploration vectors*

The textures described here from the Yerington porphyry district are most likely ubiquitous in all granitic-hydrothermal ore-forming systems. That they have been little documented is probably due to their relatively small size, poor textural preservation within the dynamic, potentially overturning, magmatic systems in which they form, limited exposure and a lack of recognition. This should not limit their use in exploration for porphyry-type mineralisation, in appropriate magmatic systems, rather we suggest that they should be sought out and considered in all field-based campaigns.

From observations of massive silica bodies and pegmatitic pods, they likely result from rapid emplacement causing intense undercooling which eventually led to fluid exsolution and periods of volatile overpressure within relatively small granitic cupolas. In the Luhr Hill granite cupola of the Yerington district, massive silica bodies and pegmatitic pods appear isolated and not directly associated with mineralisation and we regard them as being a product of undercooling. In other localities, such as at Zuun Mud (Mongolia), they are seen to transition directly into quartz USTs, and so may serve as a marker of the initial stages in the dynamic processes that lead to magmatic-hydrothermal mineralisation. In either case, porphyry-style mineralisation would likely be adjacent to or just above the massive silica bodies (Fig. 8).

Whilst many of the USTs observed in the Yerington district are unmineralised, we have also documented mineralised examples within aplite dykes. This likely indicates that the processes and conditions that led to their formation also mark the onset of magmatic-hydrothermal mineralisation associated with the aplite dykes. This is consistent with the paragenesis observed in other Au-Cu porphyry systems, for example with gold and chalcopyrite mineralisation associated with UST formation at Oyu Tolgoi as well as in porphyry Cu-Au systems of the Lachlan Fold Belt, New South Wales, Australia (Wilson, 2003; Kirwin, 2005). In many cases, therefore, USTs in the magmatic rocks that host porphyry-type mineralisation appear to provide vectors towards regions of plutons where magmas were more volatile-rich and are now relatively prospective for mineralisation. Further, our observations of USTs in the Yerington Cu-rich porphyry district illustrate that they are not restricted to Au- and Mo-rich systems, as it is likely that USTs are indicative of the physical processes (mainly rapid emplacement and hydraulic fracturing) and conditions (undercooling followed at some point by pressure fluctuations, rapid crystallisation and fluid exsolution) upon emplacement that may lead to ore formation.

Miarolitic cavities, where preserved, capture the nature and timing of fluid exsolution. Occasionally they are interconnected (e.g. Candela and Blevin, 1995; Harris et al., 2004) and/or lie within 'crystal mush dykes' (Carter et al., 2021b) and so may also be an indicator of relatively

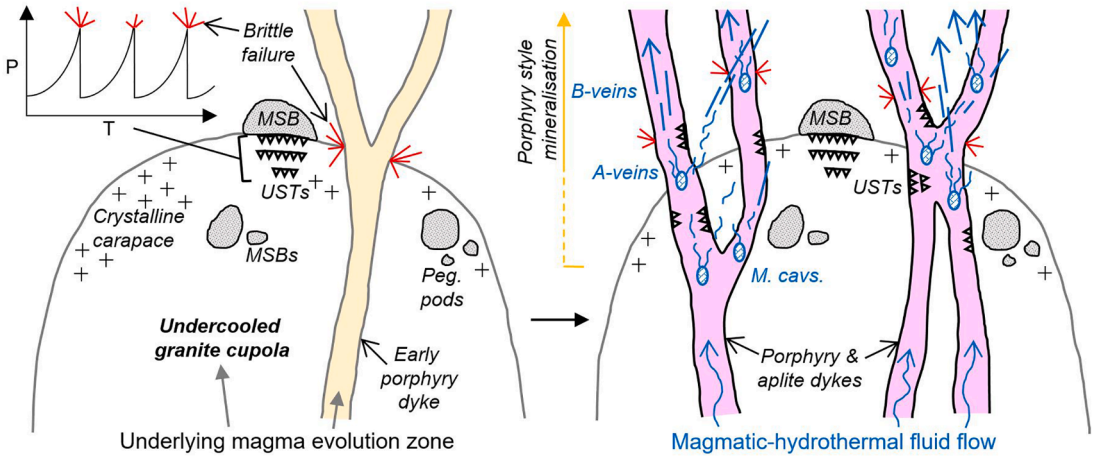

Fig. 8. Summary schematic section showing the spatial and temporal distribution of magmatic-hydrothermal textures within an undercooled granitic cupola associated with porphyry-style mineralisation. Inset graph is schematic showing pressure (P) versus time (T) during the formation of rhythmically banded USTs. Peg. pods = pegmatitic pods. MSBs = massive silica bodies (nomenclature after Kirwin, 2005). USTs = unidirectional solidification textures. M. cavs. = miarolitic cavities. A-veins represented by sinuous blue lines which transition to B-veins represented by straight blue lines. Vein nomenclature after Gustafson and Hunt (1975). Not to scale.

high levels of palaeo-permeability within immediately surrounding magmas or mush, and may signal the onset of the magmatic-hydrothermal transition. Such conditions and processes may be further evidenced from the occurrence of quartz segregations within aplite dykes, e.g. in Yerington (Fig. 3), especially where they are in close association with A- and B-type veins. Along with USTs, they would be expected to be found directly below as well as within the lower levels of porphyry-type ore deposits because they offer a snapshot of the magmatic-hydrothermal transition (Fig. 8).

In summary, the discussed textures likely formed in a continuum prior to the onset of magmatic-hydrothermal mineralisation. In the Yerington porphyry-forming magmatic system, this started with the rapid emplacement of relatively oxidised, moderately water-rich (non-H_2O saturated) Luhr Hill granite magmas to shallow (<5 km deep; Dilles, 1987) levels in the crust and consequent undercooling. That the magma did not reach fluid saturation is suggested from the anhydrous mineralogy of the massive silica bodies and pegmatitic pods, which formed within or just below the upper contact with precursor intrusives. Porphyry and aplite dykes were then episodically emplaced through the cupola region, with the presence of embayed quartz eyes likely illustrating the ease of quartz precipitation over feldspar and relatively high volatile content of the melt (Candela, 1997; Vasyukova et al., 2013). Undercooling along with repeated pressure fluctuations within the aplite dykes, due to first-type boiling (Candela, 1989) as a result of episodic hydraulic fracturing and fluid release, led to the formation of USTs ('vein dyke' texture elsewhere) prior to fluid saturation, and the later exsolution of fluids to produce miarolitic cavities. Fluid exsolution caused increased fluid pressure, the triggering of further fracturing (and reactivation of previous fractures), and the formation of quartz segregations and A-type veins. Associated pressure drops resulted in rhythmic bands of USTs. Continued upward flow of fluids through palaeo-permeability in the 'crystal mush' aplite dykes (Carter et al., 2021b), and further hydraulic fracturing throughout the system, caused a progressive evolution towards the production of AB- and B-type veins and disseminated mineralisation. These same processes occurred concurrently in vast numbers of dykes at different levels to give the complex cross-cutting relationships between dykes and vein generations typical of porphyry deposit-forming environments (Fig. 8).

5. Conclusions

We hope that this compilation of magmatic-hydrothermal disequilibrium textures in the Yerington district will aid geologists in understanding and navigating the 3D architecture of granite-related magmatic-hydrothermal ore systems. Whilst the inconsistent development or overprinting of these textures detracts from their use in some systems, in others they may provide indicators of the timing and location of the magmatic-hydrothermal transition, especially miarolitic cavities, wormy quartz segregations, USTs, massive quartz bodies and association with A- and B-type veins, and a broad indication of the location of mineralisation, usually above where they are found. Thus, they may aid in targeting in the initial stages of exploration to reduce the use of more expensive, invasive and/or environmentally impactive techniques. When combined with other geological data and observations, they can also serve as powerful tools in unravelling the intrusive history of an igneous complex.

6. Data availability

All data is available within the manuscript and its Supplementary Data files.

Declaration of Competing Interest

The authors declare that they have no known competing financial interests or personal relationships that could have appeared to influence the work reported in this paper.

Acknowledgements

This research was supported by a NERC GW4 + Doctoral Training Partnership studentship from the Natural Environment Research Council (NERC) [grant number NE/L002434/1], with additional support from the Natural History Museum, London, and British Geological Survey, and is allied to the NERC Highlight Topic project 'From Arc Magmas to Ores (FAMOS): A Mineral Systems Approach' [grant number NE/P017452/1]. We are thankful for additional funding from the SEGF's Hugh McKinstry Fund, as well as for field support and drill core access from G. Eliopulos and T. Bonsall of Quaterra Resources and M. Cunningham of Hudbay Resources (previously Mason Resources). S. Pendray, J. Anderson and G. K. Rollinson (Camborne School Mines, University of Exeter) are thanked for sample preparation, EPMA support and QEMSCAN® analysis respectively. S. Tapster (British Geological Survey), R. Armstrong, J. Wilkinson and R. Seltmann (Natural History Museum, London) are thanked along with other members of the FAMOS consortium for fruitful discussions. D. Kirwin is thanked for numerous

in-depth discussions on magmatic disequilibrium textures and for providing critical comments on this manuscript.

Appendix A. Supplementary data

Supplementary data to this article can be found online at https://doi.org/10.1016/j.oregeorev.2022.104783.

References

Baker, E.M., Andrew, A.S., 1991. Geologic, fluid inclusion, and stable isotope studies of the gold-bearing breccia pipe at Kidston, Queensland, Australia. Econ. Geol. 86 (4), 810–830.

Bryan, R. C., 2014. NI 43-101 Technical Report Mineral Resource Update Yerington Copper Project Lyon County, Nevada. TetraTech. Available: https://www.sec.gov/Archives/edgar/data/1339688/000106299314000036/exhibit99-1.htm Accessed 22/11/2021.

Candela, P.A., 1989. Felsic magmas, volatiles, and metallogenesis. In: Whitney, J.A., Naldrett, A.J. (Eds.), Ore Deposition Associated with Magmas. Reviews in Economic Geology, pp. 223–233.

Candela, P.A., 1997. A review of shallow, ore-related granites: Textures, volatiles, and ore metals. J. Petrol. 38 (12), 1619–1633.

Candela, P.A., Blevin, P.L., 1995. Do some miarolitic granites preserve evidence of magmatic volatile phase permeability? Econ. Geol. 90 (8), 2310–2316.

Carter, L. C., Tapster, S. R., Williamson, B. J. Buret, Y., Selby, D., Rollinson, G. K., Millar, I. & Parvaz, D., 2021a. An abrupt switch in magmatic plumbing taps porphyry copper deposit-forming magmas. PREPRINT (Version 1; 24 June 2021) available at Research Square. doi:10.21203/rs.3.rs-608569/v1.

Carter, L.C., Williamson, B.J., Tapster, S.R., Costa, C., Grime, G.W., Rollinson, G.K., 2021b. Crystal mush dykes as conduits for mineralising fluids in the Yerington porphyry copper district, Nevada. Commun. Earth Environ. 2, 59. https://doi.org/10.1038/s43247-021-00128-4.

Claiborne, L.L., Miller, C.F., Wooden, J.L., 2010. Trace element composition of igneous zircon: a thermal and compositional record of the accumulation and evolution of a large silicic batholith, Spirit Mountain, Nevada. Contrib. Miner. Petrol. 160 (4), 511–531. https://doi.org/10.1007/s00410-010-0491-5.

Clarke, D. E., 1969. Geology of the Ravenswood 1-mile sheet area, Queensland. Bureau of Mineral Resources, Geology and Geophysics. Record No. 1969/117.

Dilles, J.H., 1987. Petrology of the Yerington Batholith, Nevada: Evidence for evolution of porphyry copper ore fluids. Econ. Geol. 82 (7), 1750–1789.

Dilles, J.H., Einaudi, M.T., Proffett, J., Barton, M.D., 2000. Overview of the Yerington Porphyry Copper District: Magmatic to Nonmagmatic Sources of Hydrothermal Fluids, Their Flow Paths, Alteration Affects on Rocks, and Cu-Mo-Fe-Au Ores. Soc. Econ. Geol. Guidebook Series 32, 55–66. https://doi.org/10.5382/GB.32.

Dilles, J.H., Kent, A.J.R., Wooden, J.L., Tosdal, R.M., Koleszar, A., Lee, R.G., Farmer, L.P., 2015. Zircon compositional evidence for sulfur-degassing from ore-forming arc magmas. Econ. Geol. 110 (1), 241–251. https://doi.org/10.2113/econgeo.110.1.241.

Dilles, J. H. & Proffett, J. M., 1995. Metallogenesis of the Yerington batholith, Nevada. *In:* Pierce, F. W., & Bolm, J. G. (Eds.), Porphyry copper deposits of the American cordillera: Arizona Geological Society Digest, 20, pp. 306–315.

Dilles, J.H., Wright, J.E., 1988. The chronology of early Mesozoic arc magmatism in the Yerington district of western Nevada and its regional implications. Geol. Soc. Am. Bull. 100 (5), 644–652.

Erdenebayar, J., Ogata, T., Imai, A., Sereenen, J., 2014. Textural and chemical evolution of unidirectional solidification textures in highly differentiated granitic rocks at Kharaatyagaan, Central Mongolia. Resource Geol. 64 (4), 283–300.

Fenn, P.M., 1986. On the origin of graphic granite. Am. Mineral. 71 (4), 325–330.

Garwin, S., 2002. The geology of intrusion-related hydrothermal systems near the Batu Hijau porphyry coper-gold deposit, Sumbawa, Indonesia. *In:* Goldfarb, R. & Nielsen, R. (eds.), Integrated Methods for Discovery. Reviews in Economic Geology, Special Publication 9, pp. 333-366.

Goodall, W.R., Scales, P.J., Butcher, A.R., 2005. The use of QEMSCAN and diagnostic leaching in the characterisation of visible gold in complex ores. Miner. Eng. 18 (8), 877–886. https://doi.org/10.1016/j.mineng.2005.01.018.

Goodall, W.R., Scales, P.J., 2007. An overview of the advantages and disadvantages of the determination of gold mineralogy by automated mineralogy. Miner. Eng. 20 (5), 506–517. https://doi.org/10.1016/j.mineng.2007.01.010.

Gottlieb, P., Wilkie, G., Sutherland, D., Ho-Tun, E., Suthers, S., Perera, K., Jenkins, B., Spencer, S., Butcher, A., Rayner, J., 2000. Using quantitative electron microscopy for process mineralogy applications. JOM 52 (4), 24–25. https://doi.org/10.1007/s11837-000-0126-9.

Gustafson, L.B., Hunt, J.P., 1975. The porphyry copper deposit at El Salvador, Chile. Econ. Geol. 70 (5), 857–912.

Halley, S., Dilles, J.H., Tosdal, J.H., 2015. Footprints: Hydrothermal Alteration and Geochemical Dispersion Around Porphyry Copper Deposits. SEG Newsletter 100, 12–17.

Harris, A. C., Cuison, A. L. G., Chang, Z., Cooke, D. R., Bonnici, N., Faure, K. & Cross, C., 2007. Fe-rich magmatic volatiles in the Ridgeway Au-Cu porphyries: evidence from magnetite-quartz comb-layered textures. *In*: C. J. Andrew (Ed.), Digging Deeper, Proceedings of the 9th Biennial SGA Meeting, Dublin. pp. 415–418.

Harris, A.C., Kremenetsky, V.S., White, N.C., Steele, D.A., 2004. Volatile phase separation in silic magmas at Bajo de la Alumbrera porphyry Au-Cu deposit NW Argentina. Resour. Geol. 54, 341–356.

Henderson, M. R., Bryan, R. C., Welhener, H. E., Jolk, R. W. & Willow, M. A., 2014. MacArthur Copper Project; Amended NI 43-101 Technical Report Preliminary Economic Assessment. M3 Engineering. Available: https://quaterra.com/download/macarthur-pea-technical-report-january-2014/ Accessed 04/10/2021.

Hithersay, P.S., Walshe, J.L., 1995. Endeavour 26 North: a porphyry copper-gold deposit in the Late Ordovician shoshonite Goonumbla volcanic complex, New South Wales, Australia. Econ. Geol. 90, 1506–1532.

Hong, W., Cooke, D.R., Zhang, L., Fox, N., Thompson, J., 2019. Cathodoluminescence features, trace elements, and oxygen isotopes of quartz in unidirectional solidification textures from the Sn-mineralized Heemskirk Granite, western Tasmania. Am. Mineral. 104, 100–117.

Hudbay Minerals Inc. Mason Preliminary Economic Assessment Summary, 2021. Available: https://hudbayminerals.com/investors/press-releases/press-release-details/2021/Hudbay-Announces-Positive-Preliminary-Economic-Assessment-for-its-Mason-Copper-project/default.aspx Accessed 04/10/2021.

Hudson, D.M., Oriel, W.M., 1979. Geologic map of the Buckskin Range, Nevada, 64. Nevada Bureau of Mines and Geology, map.

Kelly, W.C., Rye, R.O., 1979. Geologic, fluid inclusion, and stable isotope studies of the tin–tungsten deposits of Panasqueira, Portugal. Econ. Geol. 74 (8), 1721–1822.

Kirkham, R.V., Sinclair, W.D., 1988. *In:* Taylor, R. P., Strong, D. F. (Eds.), Recent advances in the geology of granite-related mineral deposits. Canadian Institute of Mining, Special Volume 31, pp. 50–71.

Kirwin, D.J., 2005. Unidirectional solidification textures associated with intrusion-related Mongolian mineral deposits. In: Seltmann, R., Gerel, O., Kirwin, D.J. (Eds.), Geodynamics and metallogeny of Mongolia with special emphasis on copper and gold deposits: Society of Economic Geologists-International Association for the Genesis of Ore Deposits Field Trip, 2005: IAGOD Guidebook Series 11: London. Centre for Russian and Central EurAsian Mineral Studies, Natural History Museum, pp. 63–84.

Kronz, A., Van den Kerkhof, A.M., Müller, A., 2012. Analysis of Low Element Concentrations in Quartz by Electron Microprobe. In: Götze, J., Möckel, R. (Eds.), Quartz: Deposits, Mineralogy and Analytics. Springer Geology. Springer, Berlin, Heidelberg. https://doi.org/10.1007/978-3-642-22161-3_9.

London, D., 1992. The application of experimental petrology to the genesis and crystallisation of granitic pegmatites. Can. Mineral. 30, 499–540.

London, D., 2009. The origin of primary textures in granitic pegmatites. Can. Mineral. 47 (4), 697–724.

London, D., Morgan, G.B., 2012. The pegmatite puzzle. Elements 8 (4), 263–268.

McDowell, S.M., Miller, C.F., Mundil, R., Ferguson, C.A., Wooden, J.L., 2014. Zircon evidence for a ~200 k.y. supereruption-related thermal flare-up in the Miocene southern Black Mountains, western Arizona, USA. Contrib. Miner. Petrol. 168, 1031. https://doi.org/10.1007/s00410-014-1031-5.

Müller, A., Herrington, R., Armstrong, R., Seltmann, R., Kirwin, D.J., Stenina, N.G., Kronz, A., 2010. Trace elements and cathodoluminescence of quartz in stockwork veins of Mongolian porphyry-style deposits. Miner. Deposita 45 (7), 707–727.

Mustard, R., Neilsen, R., Ruxton, P.A., 1988. Timbarra gold deposits. In: Berkman, D.A., Mackenzie, D.H. (Eds.), Geology of Australia and Papua New Guinea Mineral deposits. Australian Institute of Mining and Metallurgy, Melbourne, pp. 551–560.

Proffett, J.M., 1977. Cenozoic geology of the Yerington district, Nevada, and implications for the nature and origin of Basin and Range faulting. GSA Bull. 88 (2), 247–266.

Proffett, J.M., 1979. Ore deposits of the western United States: A summary. In: Ridge, J. D. (Ed.), Papers on Mineral Deposits of Western North America, 33. Nevada Bureau of Mines and Geology, pp. 13–32.

Proffett, J.M., 2007. Report on the geology and genesis of the Yerington porphyry copper district, Nevada, a four dimensional study. Final report for: USGS mineral resource external research program grant 06HQGR0171.

Proffett, J.M., Dilles, J.H., 1984. Geological map of the Yerington district. Nevada Bureau of Mines and Geology, Nevada map 77.

Richards, J. P., 2005. Cumulative factors in the generation of giant calc-alkaline porphyry Cu deposits. *In:* Porter, T.M. (ed.), Super porphyry copper and gold deposits: A global perspective, v. 1: Adelaide, PGC Publishing, pp. 7−25.

Richards, J. P., 2011. High Sr/Y arc magmas and porphyry Cu±Mo±Au deposits: Just add water. Economic Geology, 106(7), pp. 2075-1081. doi:10.2113/econgeo.106.7.1075.

Rohrlach, B., Loucks, R., 2005. Multi-million-year cyclic ramp-up of volatiles in a lower crustal magma reservoir trapped below the Tampakan copper-gold deposit by Mio-Pliocene crustal compression in the southern Philippines. Adelaide, PGC Publ. 2, 369–407.

Rollinson, G.K., Andersen, J.C.Ø., Stickland, R.J., Boni, M., Fairhurst, R., 2011. Characterisation of non-sulphide zinc deposits using QEMSCAN®. Miner. Eng. 24 (8), 778–787. https://doi.org/10.1016/j.mineng.2011.02.004.

Rombach, C.S., Newberry, R.J., 2001. Shotgun deposit: granite porphyry-hosted gold-arsenic mineralisation in southwestern Alaska, USA. Miner. Deposita 36, 607–621.

Runyon, S.E., Steele-MacInnis, M., Seedorff, E., Lecumberri-Sanchez, P., Mazdab, F.K., 2017. Coarse muscovite veins and alteration deep in the Yerington batholith, Nevada: insights into fluid exsolution in the roots of porphyry copper systems. Miner. Deposita 52 (4), 463–470. https://doi.org/10.1007/s00126-017-0720-1.

Schöpa, A., Annen, C., Dilles, J.H., Sparks, R.S.J., Blundy, J.D., 2017. Magma emplacement rates and porphyry copper deposits: Thermal modeling of the Yerington Batholith, Nevada. Econ. Geol. 112, 1653–1672.

Seedorff, E., Barton, M.D., Stavast, W.J.A., Maher, D.J., 2008. Root Zones of Porphyry Systems: Extending the Porphyry Model to Depth. Econ. Geol. 103 (5), 939–956.

Shannon, J.R., Walker, B.M., Carten, R.B., Geraghty, E.P., 1982. Unidirectional solidification textures and their significance in determining relative ages of intrusions at the Henderson Mine, Colorado. Geology 10 (6), 293. https://doi.org/10.1130/0091-7613(1982)10<293:USTATS>2.0.CO;2.
Sillitoe, R.H., 2010. Porphyry Copper Systems. Econ. Geol. 105 (1), 3–41.
Spurr, J.E., 1923. The ore magmas. McGraw-Hill, New York, p. 915.
Swanson, S.E., 1977. Relation of nucleation and crystal-growth rate to the development of granitic textures. Am. Mineral. 62, 966–978.
Terzaghi, K., Peck, R.B., 1948. Soil Mechanics in Engineering Practice. John Wiley & Sons, New York.
Tungalag, N., Jargalan, S., Khashgerel, B.-E., Mijiddorj, C., Kavalieris, I., 2018. Characteristics of the Late Devonian Tsagaan Suvarga Cu-Mo deposit, Southern Mongolia. Miner. Deposita 54 (3), 369–380.
Tuttle, O.F., Bowen, N.L., 1958. Origin of granite in the light of experimental studies in the system NaAlSi3O8-KAlSi3O8-SiO,-H. O. Geol. Soc. Am. Memoir 74, 153.
Vasyukova, O.V., Goemann, K., Kamenetsky, V.S., MacRae, C.M., Wilson, N.C., 2013. Cathodoluminescence properties of quartz eyes from porphyry-type deposits: Implications for the origin of quartz. Am. Mineral. 98 (1), 98–109. https://doi.org/10.2138/am.2013.4018.
Wark, D.A., Watson, E.B., 2006. TitaniQ: a titanium-in-quartz geothermometer. Contrib. Miner. Petrol. 152 (6), 743–754.
White, W.H., Bookstrom, A.A., Kamilli, R.J., Ganster, M.W., Smith, R.P., Ranta, D.E., Steininger, R.C., 1981. Character and origin of Climax-type molybdenum deposits: Economic Geology. In: 75th Anniversary Volume, pp. 270–316.
Wilkinson, J.J., 2013. Triggers for the formation of porphyry deposits in magmatic arcs. Nat. Geosci. 6, 917–925.
Wilson, A.J., 2003. The geology, genesis and exploration context of the Cadia gold-copper porphyry deposits. University of Tasmania, New South Wales, Australia. PhD thesis.